Science Advances
AAAS

advances.sciencemag.org/cgi/content/full/7/7/eabe0579/DC1

Supplementary Materials for

Wireless, implantable catheter-type oximeter designed for cardiac oxygen saturation

Wei Lu, Wubin Bai, Hao Zhang, Chenkai Xu, Antonio M. Chiarelli, Abraham Vázquez-Guardado, Zhaoqian Xie, Haixu Shen, Khizar Nandoliya, Hangbo Zhao, KunHyuck Lee, Yixin Wu, Daniel Franklin, Raudel Avila, Shuai Xu, Alina Rwei, Mengdi Han, Kyeongha Kwon, Yujun Deng, Xinge Yu, Edward B. Thorp, Xue Feng, Yonggang Huang, Joseph Forbess, Zhi-Dong Ge*, John A. Rogers*

*Corresponding author. Email: zhi-dong.ge@northwestern.edu (Z.-D.G.); jrogers@northwestern.edu (J.A.R.)

Published 10 February 2021, *Sci. Adv.* **7**, eabe0579 (2021)
DOI: 10.1126/sciadv.abe0579

This PDF file includes:

Figs. S1 to S20

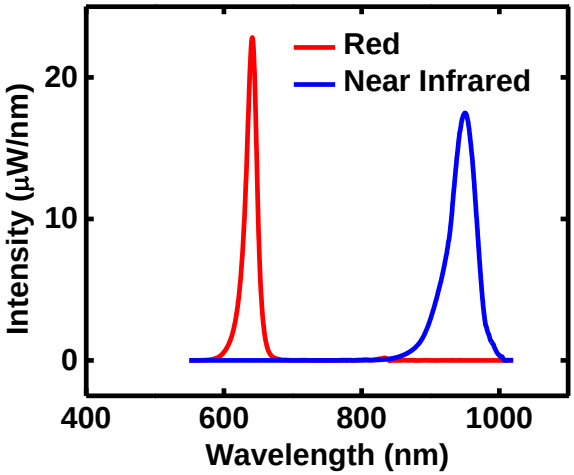

Fig. S1. Measured spectra for the red and near-infrared (NIR) LEDs of the sensing probes. The measured spectral bandwidths are ~34 nm and ~53 nm for red and NIR LED, respectively.

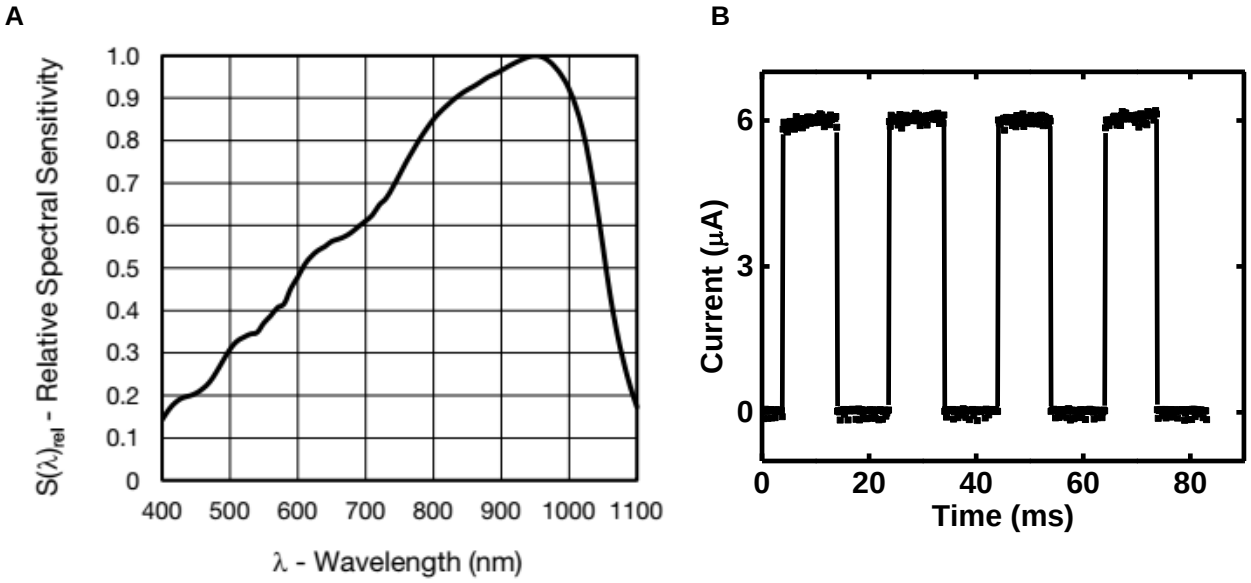

Fig. S2. Photoelectric characterization of the miniaturized photodiode. (A) Relative spectral sensitivity vs. wavelength. **(B)** Measured photocurrent from the photodiode at the sensing probe as a function of time for illumination with light after passing through a chopper (red light, wavelength: 633 nm; optical power: 4 mW).

A

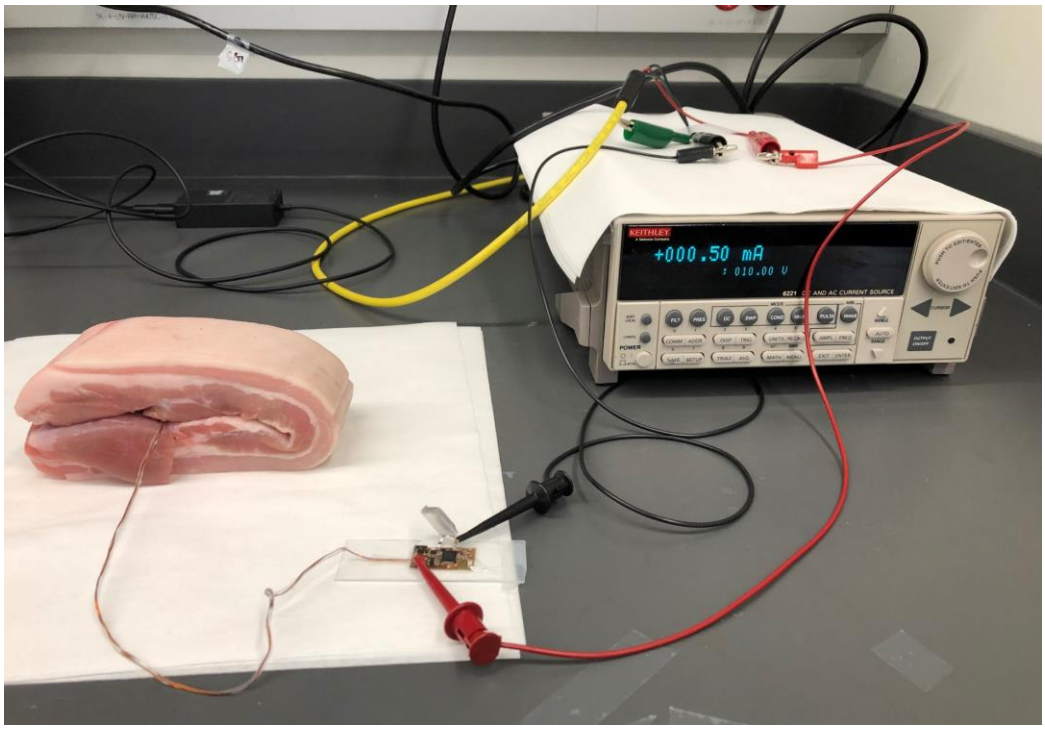

B

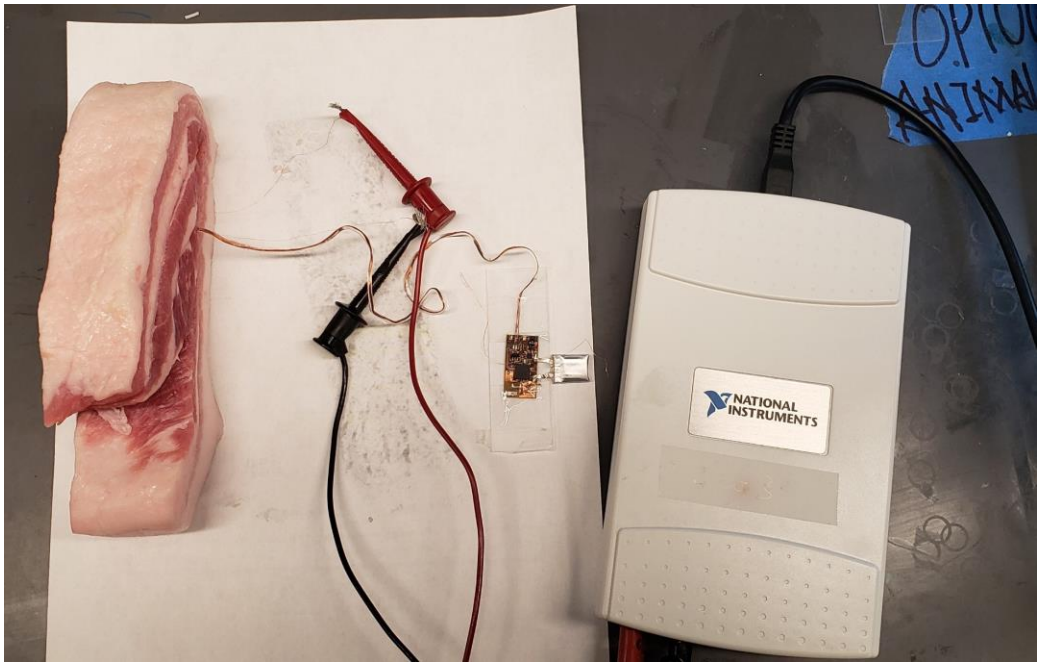

Fig. S3 Test platforms for measuring the optical response and thermal characteristics of the catheter oximeter probe. (A) Test platform for measuring NIR and RED LED optical responses, for Fig. 2B. **(B).** Test platform for measuring the thermal characteristics of the catheter oximeter probe, for Fig. 2E. (Photo credit: Wei Lu and Haixu Shen, Northwestern University)

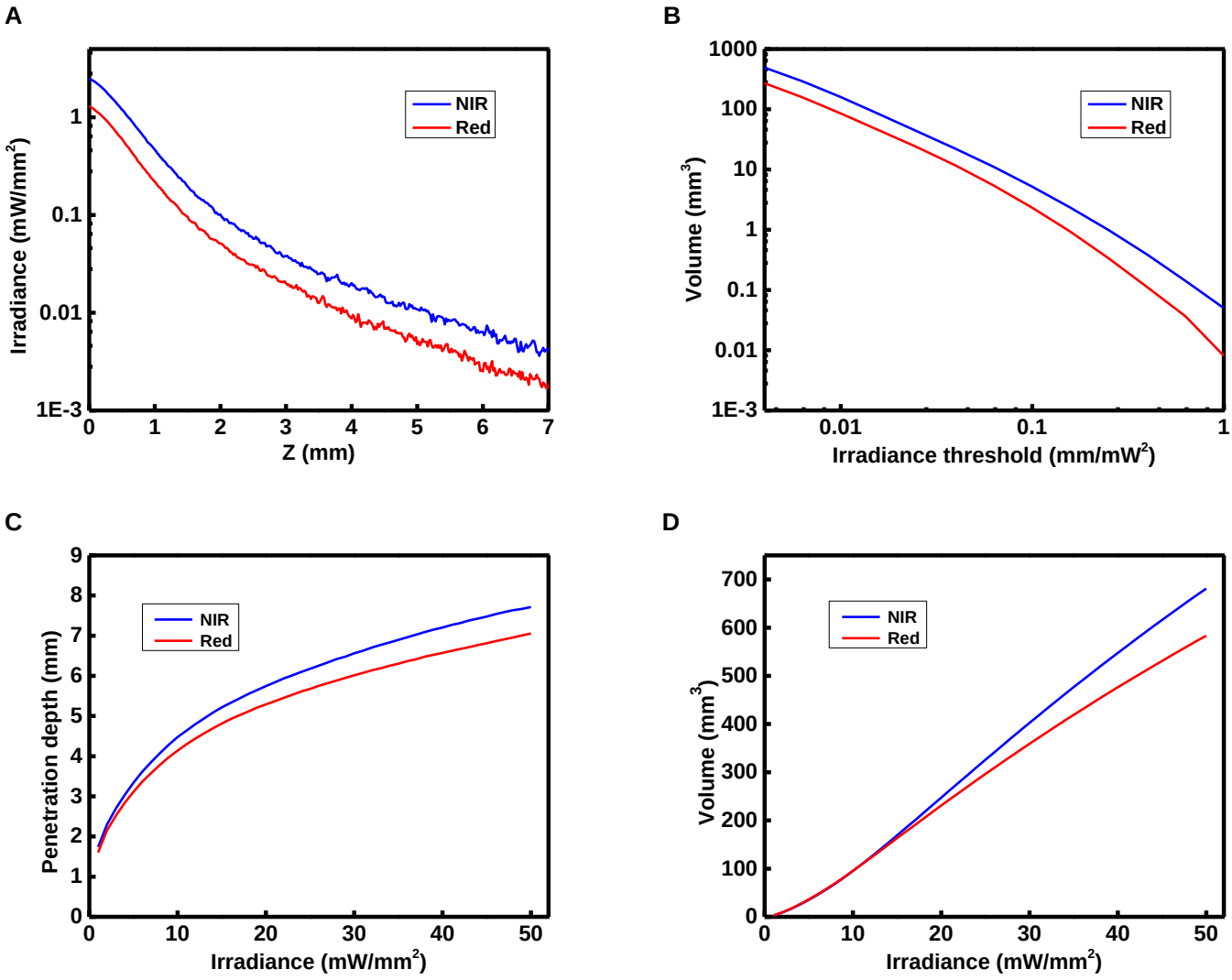

Fig. S4. Monte Carlo simulation of the optical characteristics. (A) Light intensity decay from catheter/muscle boundary, along the z-axis right on top of red LED and NIR LED respectively; **(B)** The illumination volume in cardiac tissue for red and NIR LEDs as a function of irradiance threshold. **(C)** Light penetration depth in tissue as a function of LED irradiance, for threshold 0.01 mW/mm^2; **(D)** Light illumination volume in tissue as a function of LED irradiance, for threshold of 0.01 mW/mm^2.

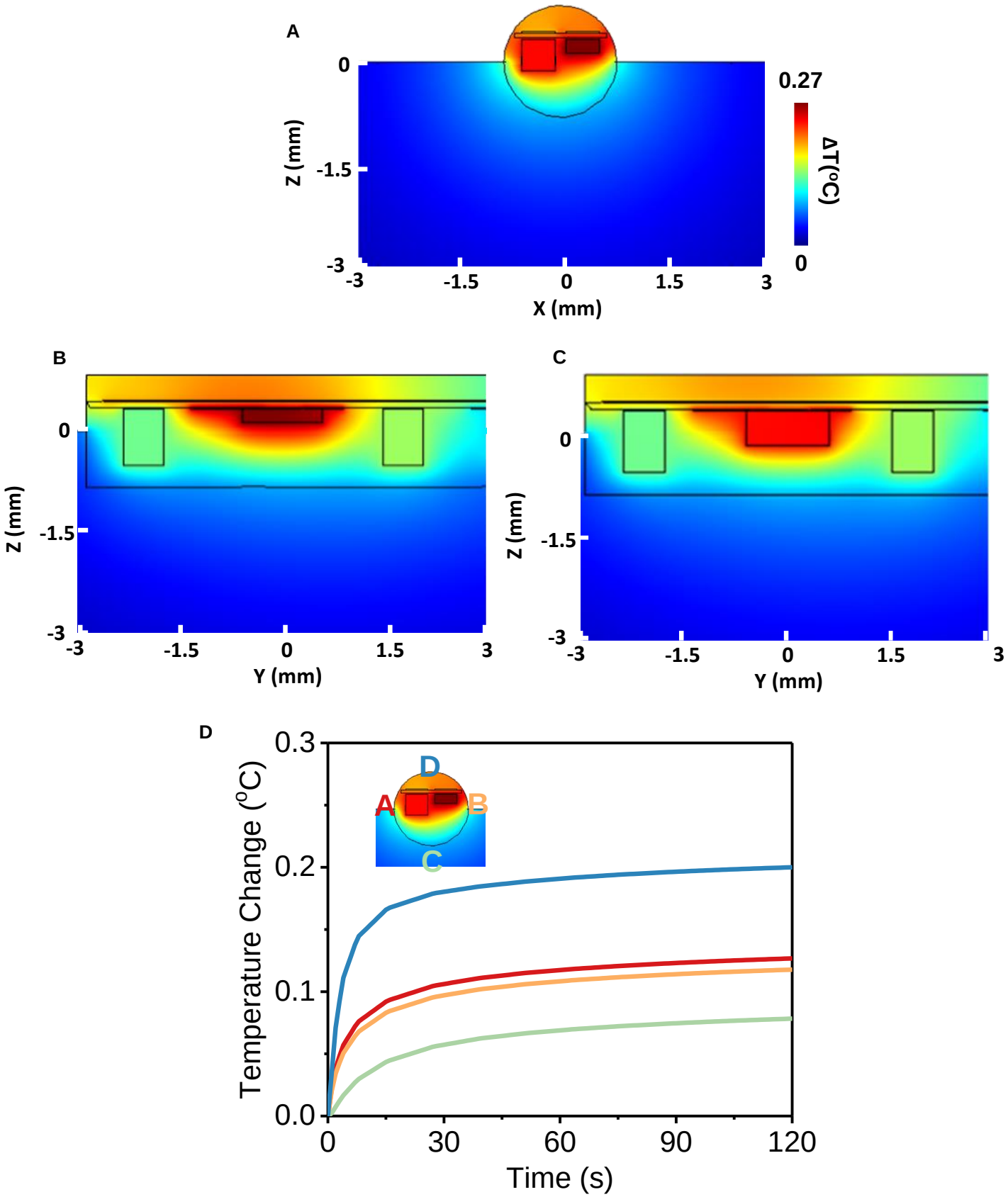

Fig. S5. Finite Element Analysis (FEA) results of temperature change in the tissue and catheter probe after the probe operation of 120 s. (A) Temperature change distribution in the ZX plane at the middle (Y = 0 mm) of the Red and NIR LEDs. **(B)** Temperature change distribution in the ZY plane at the middle (X = 0.3 mm) of the Red LEDs. **(C)** Temperature change distribution in the ZY plane at the middle (X = - 0.3 mm) of the NIR LED. **(D)** Temperature change distribution as a function of time of four representative points (A, B, C, D) in proximity with the LEDs. Maximum temperature change based on FEA is 0.2 ℃.

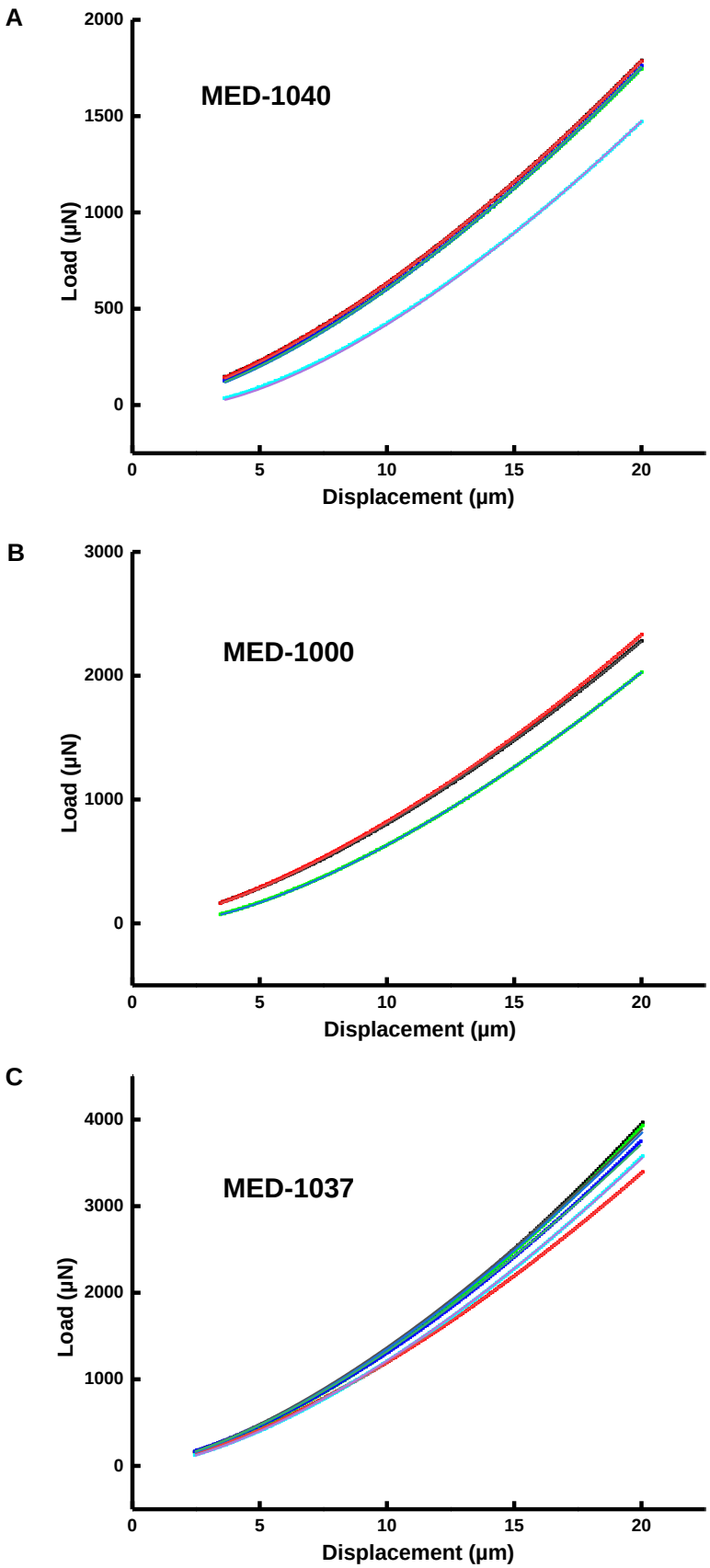

Fig. S6. Load-displacement curves from indentation tests on three different bio-compatible silicone materials. (A) MED-1040, **(B)** MED-1000, **(C)** MED-1037.

A

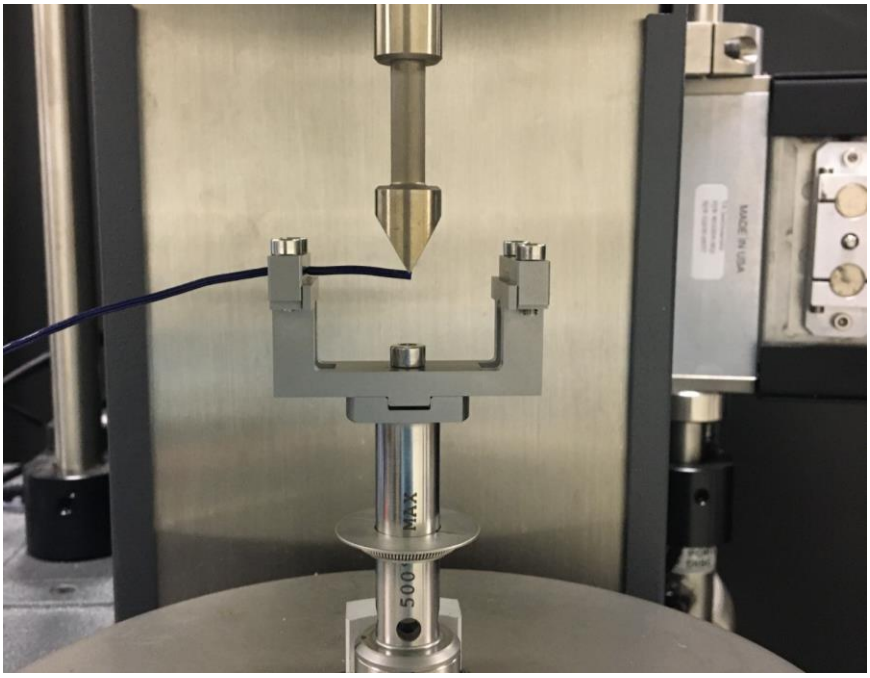

B

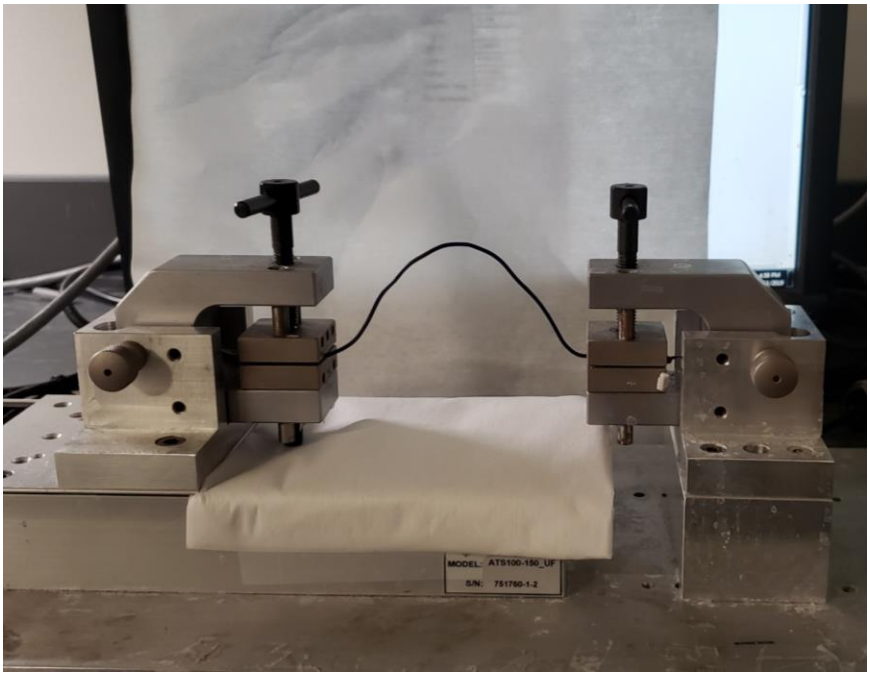

Fig. S7. Test platforms for measuring the mechanical properties of the catheter oximeter probe. **(A)** Dynamic mechanical tester setup for measuring the bending stiffness of catheter probes. **(B)** Test platform for measuring the catheter oximeter probe during bending and stretching, for Fig. 3E. (Photo credit: Hangbo Zhao and Wei Lu, Northwestern University)

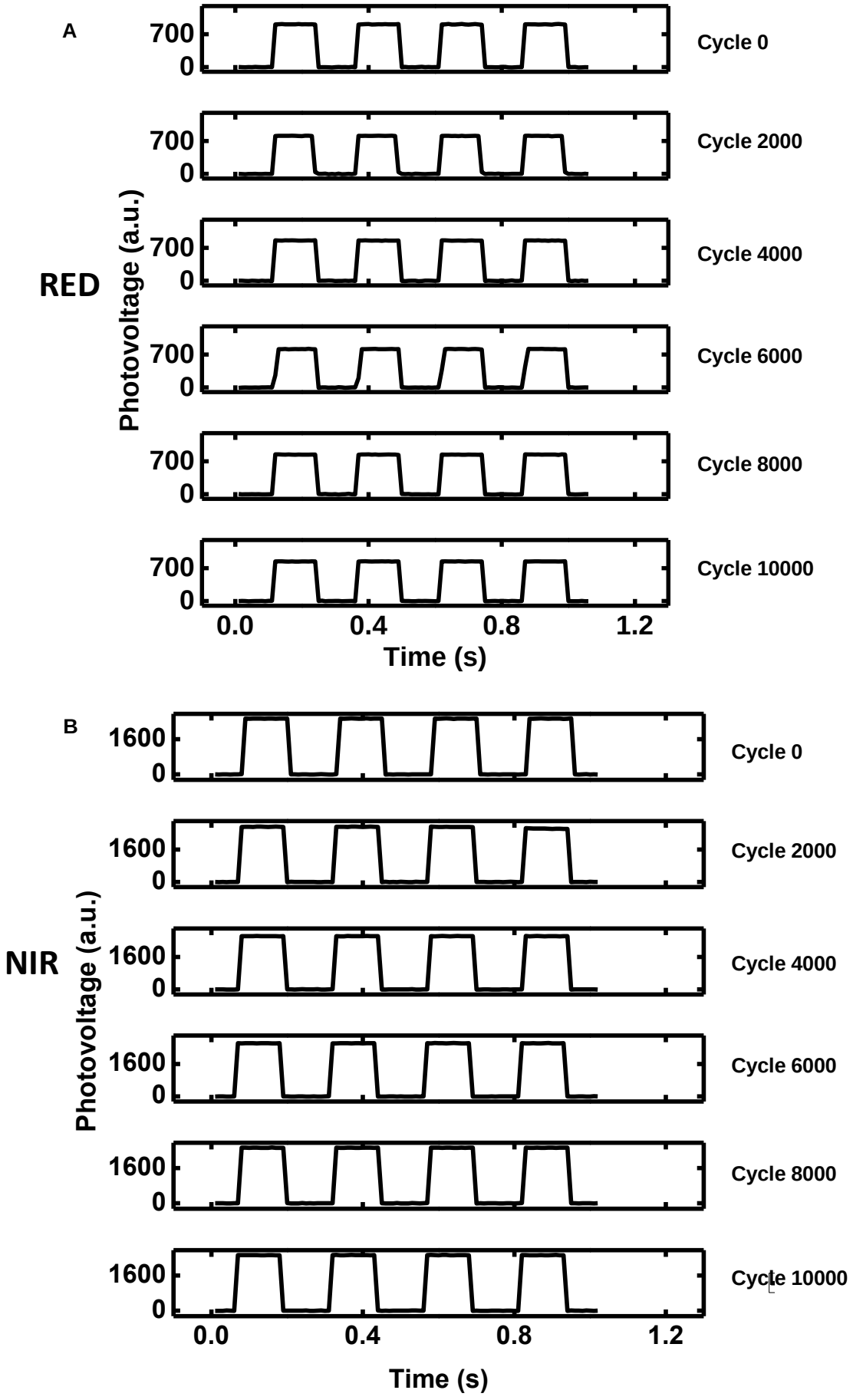

Fig. S8. Pulse signal emitted by the LED and measured by the photodiode, with catheter oximeter probe in different stretch cycles. (A) Red and **(B)** NIR LED pulse signal in different stretch cycles.

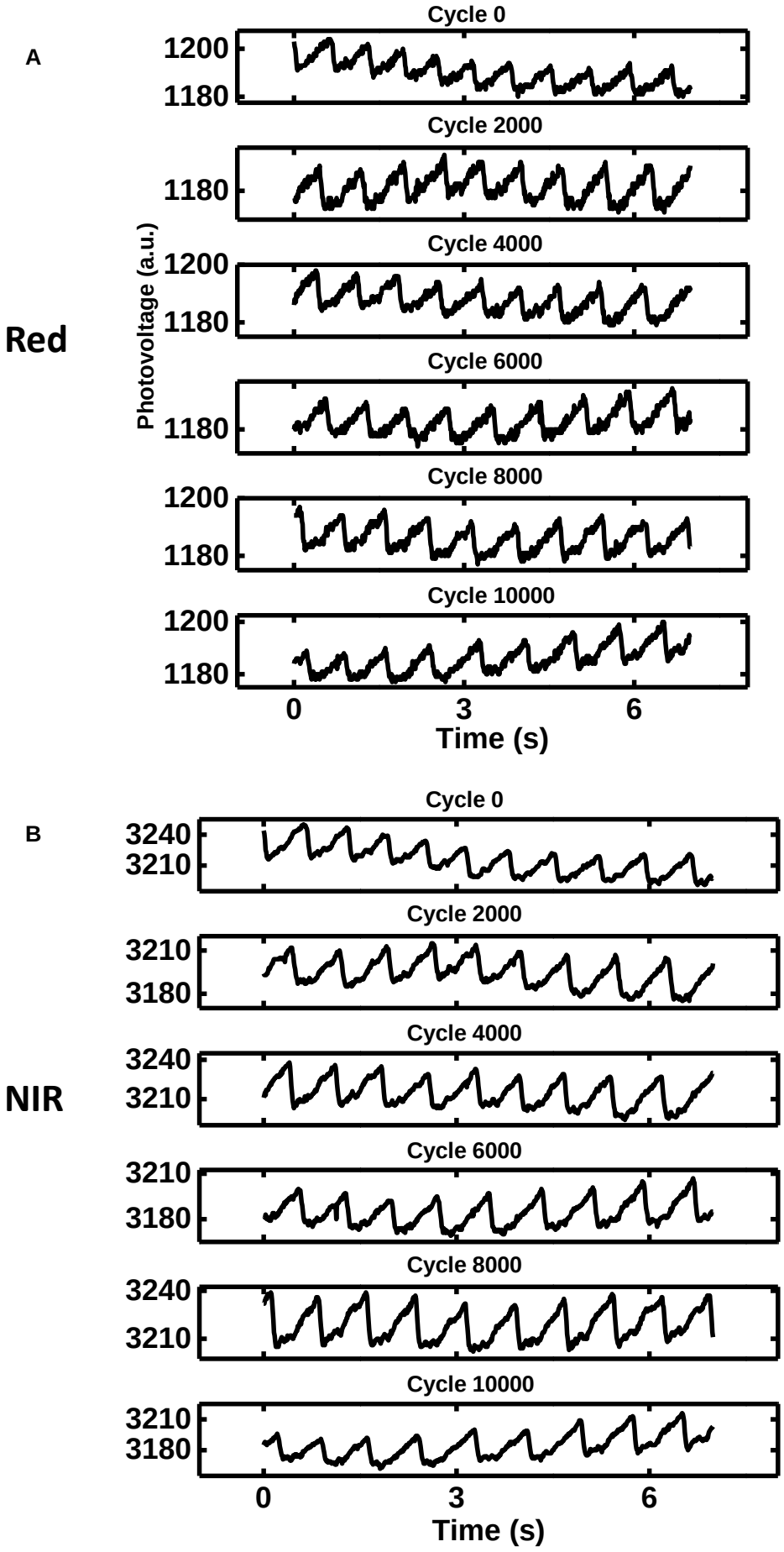

Fig. S9. Measured human pulse signal by wireless catheter oximeter, with the catheter probe after different stretch cycles. Human pulse signal from **(A)** Red, **(B)** NIR LEDs respectively.

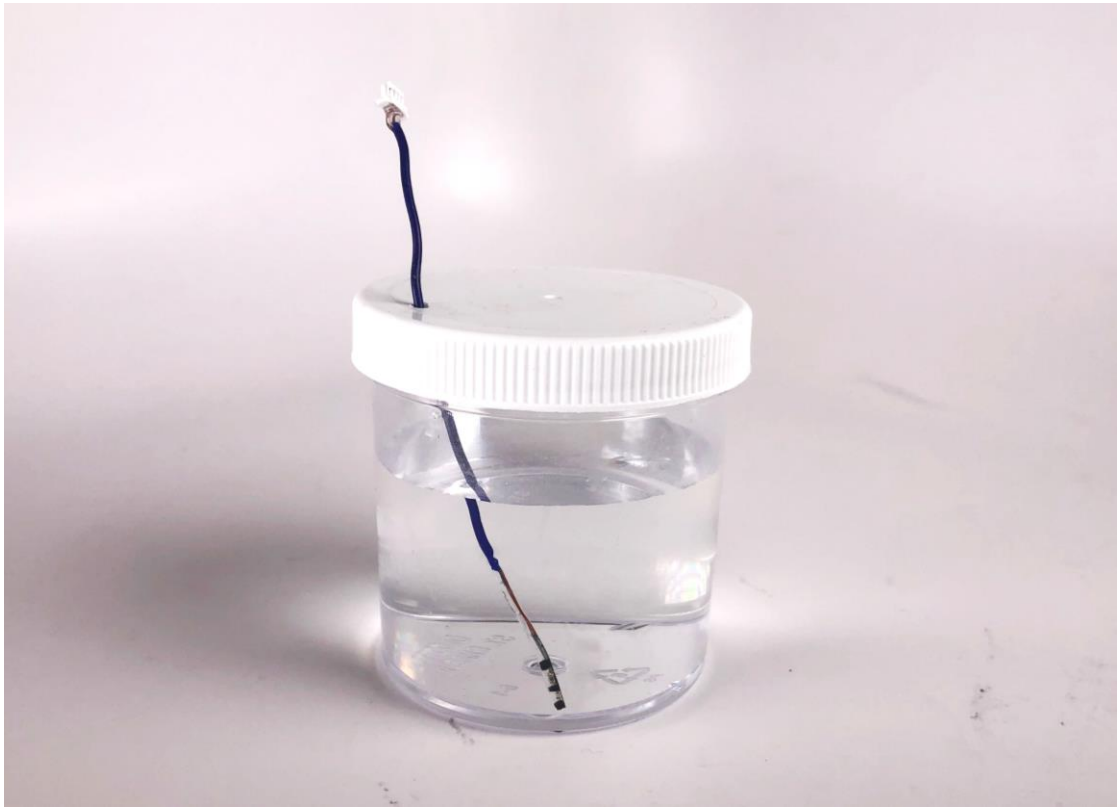

Fig. S10. Image of the setup for the phosphate-buffered saline (PBS) soak test. The catheter oximeter probe is immersed in PBS solution. The entire system is placed inside an oven at 37 ℃. (Photo credit: Wubin Bai, Northwestern University)

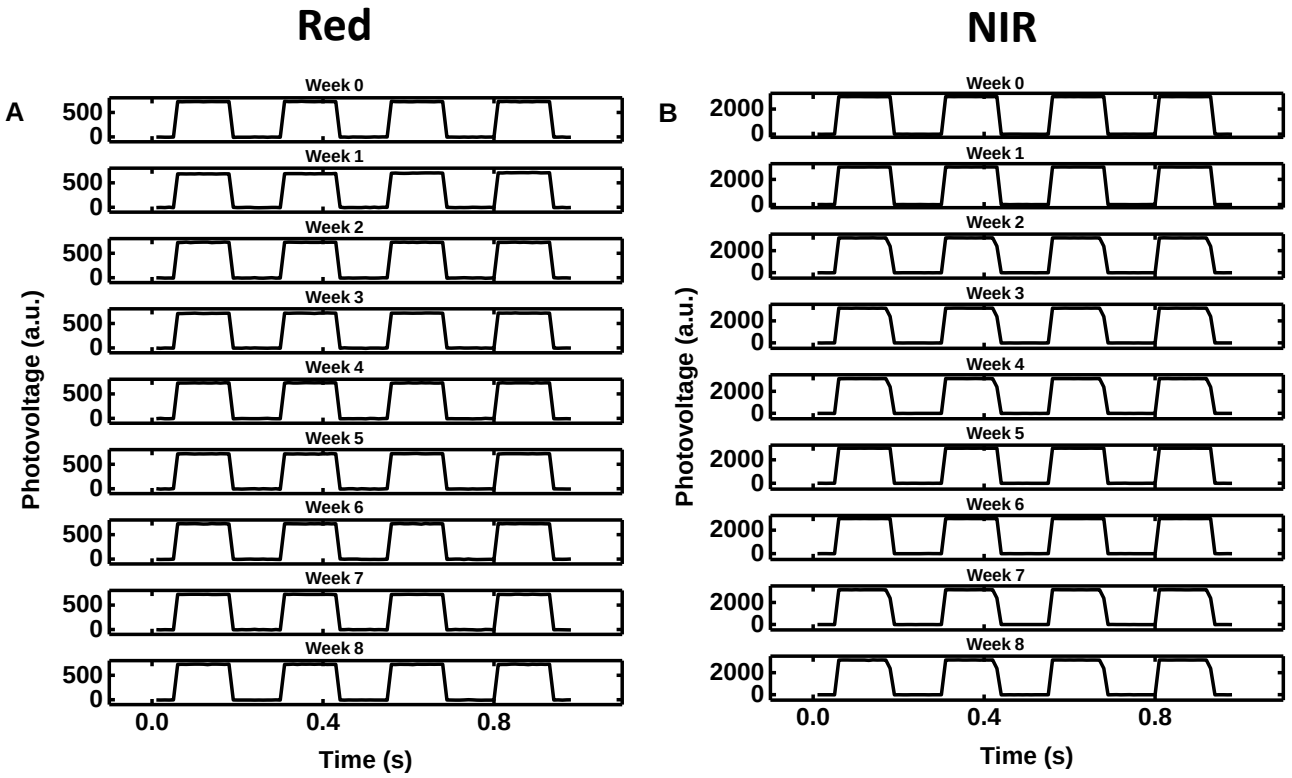

Fig. S11. Pulsed emission from the LEDs and measured by the photodiode, with a catheter oximeter probe immersed for different times in phosphate-buffered saline (PBS) solution at 37 °C. (A) Red and **(B)** NIR LED pulse signal at different immersion time.

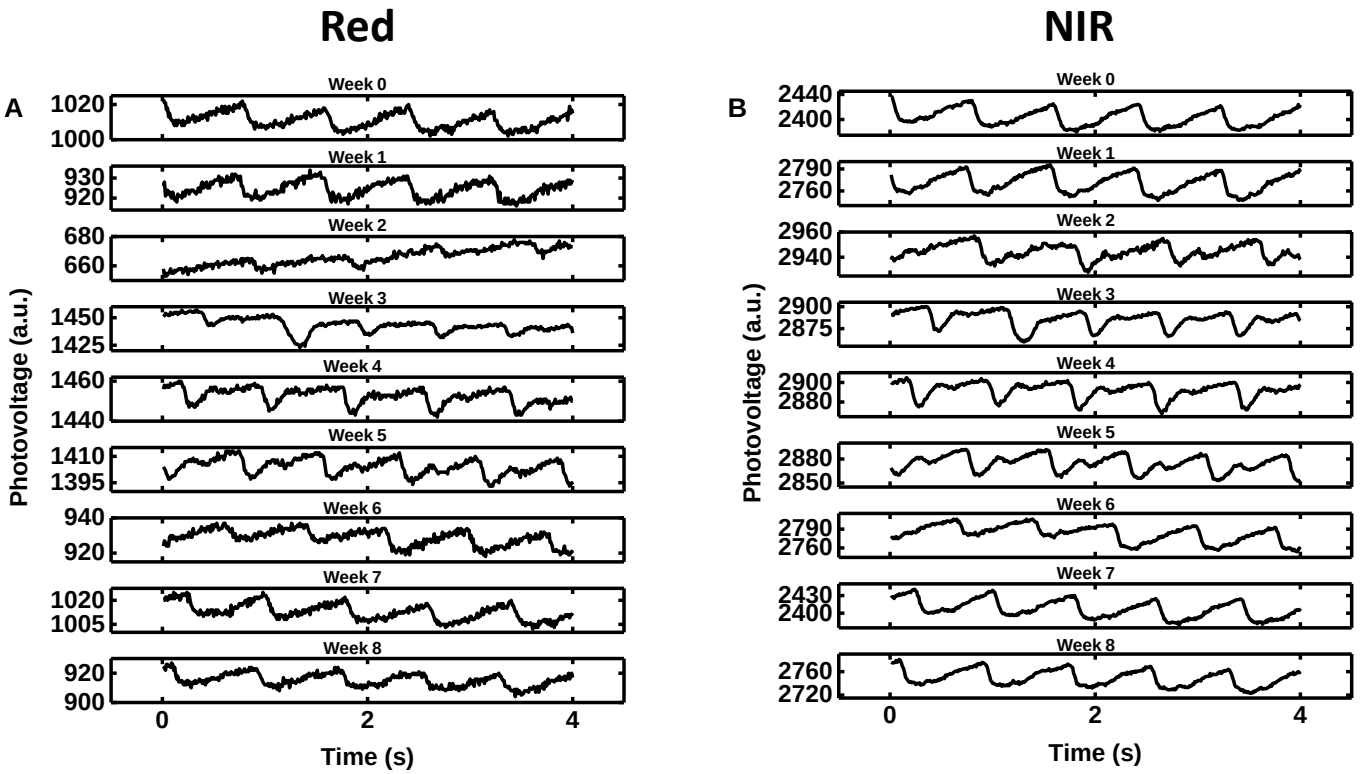

Fig. S12. Measured human pulse signal captured by wireless catheter oximeter, with the catheter probe immersed for different times in phosphate-buffered saline (PBS) solution at 37 °C. Human pulse signal from **(A)** Red, **(B)** NIR LEDs respectively.

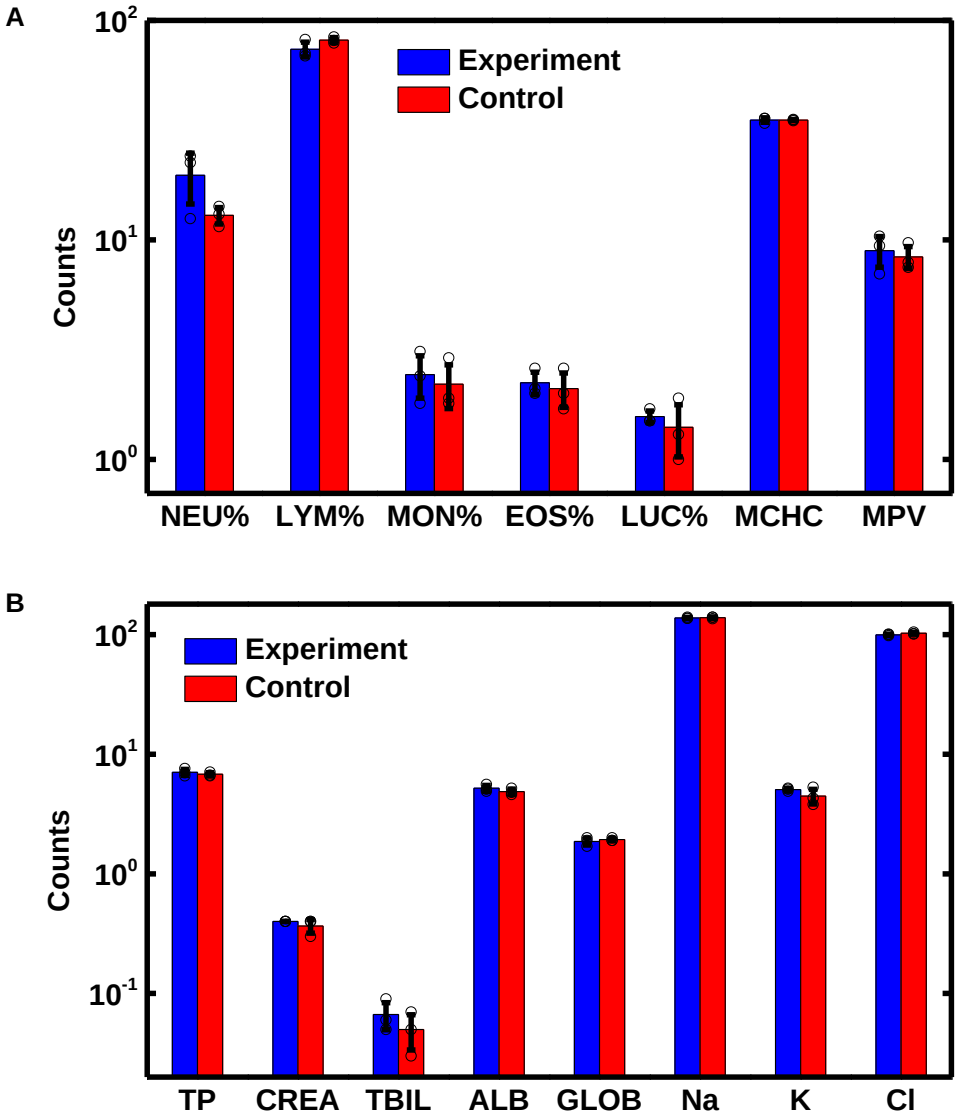

Fig. S13. Analysis of complete blood count and blood chemistry for the mice with catheter oximeter probe implanted subcutaneously for 30 days (labeled as Experiment) and the mice without device implantation (labeled as Control). (A) Blood count. **(B)** Blood chemistry.

Abbreviations and corresponding units include, WBC: white blood cell (K/μL), RBC: red blood cell (M/μL), HGB: blood hemoglobin level (g/dL), HCT: hematocrit level (%), MCV: mean corpuscular volume (fL), MCH: mean corpuscular hemoglobin (pg), RDW: red cell distribution width (%), PLT: platelet count in blood (L/μL), GLU: glucose (mg/dL), TRIG: triglycerides (mg/dL), ALT: alanine aminotransferase (U/L), AST: aspartate transaminase (IU/L), ALP: alkaline phosphatase (IU/L), CHOL: cholesterol (mg/dL), PHOS: phosphorus (mg/dL), CAL: calcium (mg/dL), NEU%: percentage of neutrophils (%), LYM%: percentage of lymphocytes (%), MON%: percentage of monocytes (%), EOS%: percentage of eosinophils (%), LUC%: percentage of large unstained cells (%), MCHC: mean corpuscular hemoglobin concentration (g/dL), MPV: mean platelet volume (fL), TP: total protein (g/dL), CREA: creatinine (mg/dL), TBIL: total bilirubin level (mg/dL), ALB: albumin (g/dL), GLOB: globulin (g/dL), Na: sodium (mEq/L), K: potassium (mEq/L), Cl: chloride (mEq/L).

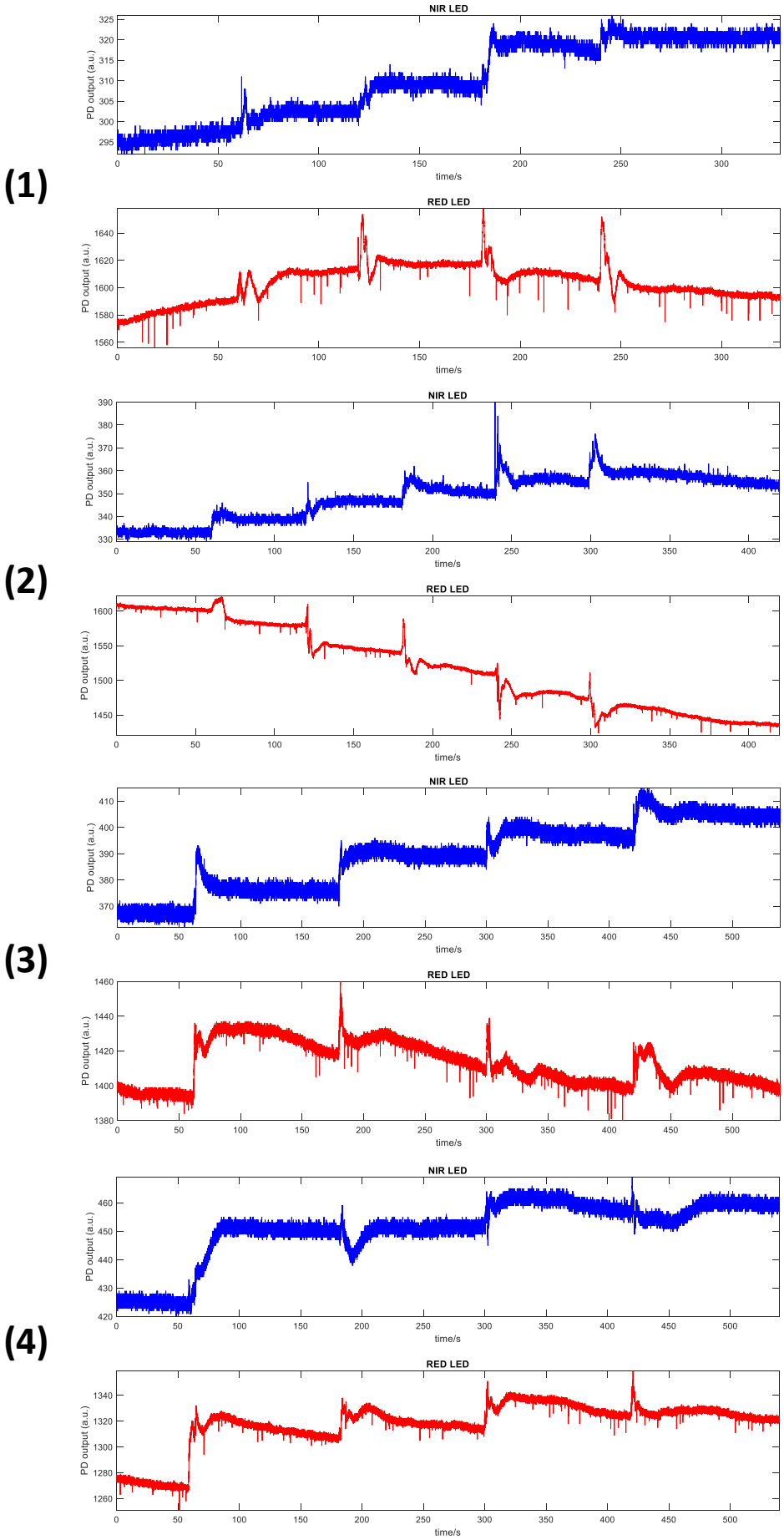

Fig. S14. Raw data recorded from a wireless catheter oximeter in blood with time varying Hb/HbO, with comparison to measurements performed with a commercial (Edwards) oximeter.

A

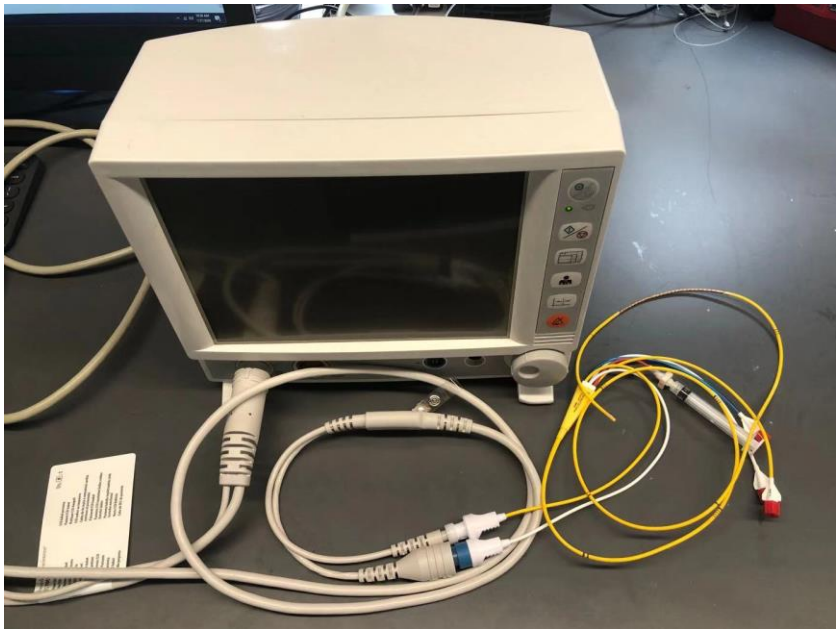

B

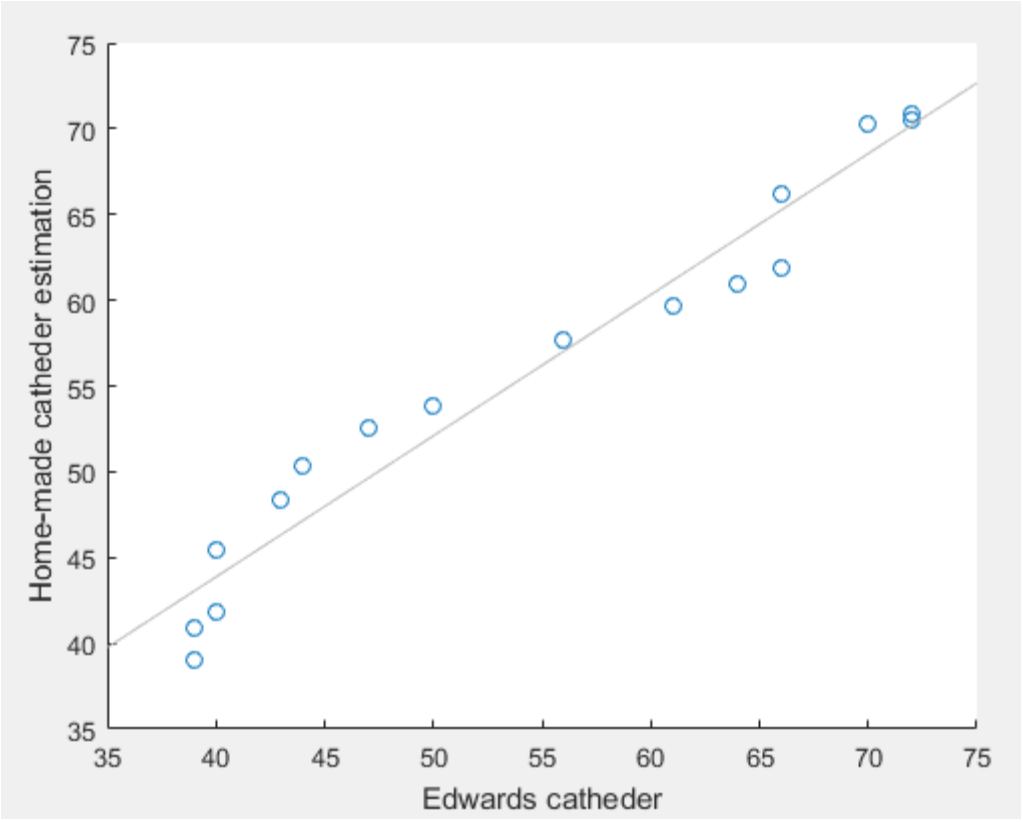

Fig. S15. Commercial fiber optic catheter oximeter system, and the in vitro comparison test between this system and the wireless catheter oximeter. (A) Image shows the fiber optic catheter and the monitoring machine (Edwards). **(B)** In vitro test of calculated blood oxygen saturation derived from measurements with a wireless catheter oximeter, with comparison to measurements performed with a commercial fiber optic oximeter (Swan Ganz 777F8, and HemoSphere advanced monitoring platform). (Photo credit: Wei Lu , Northwestern University)

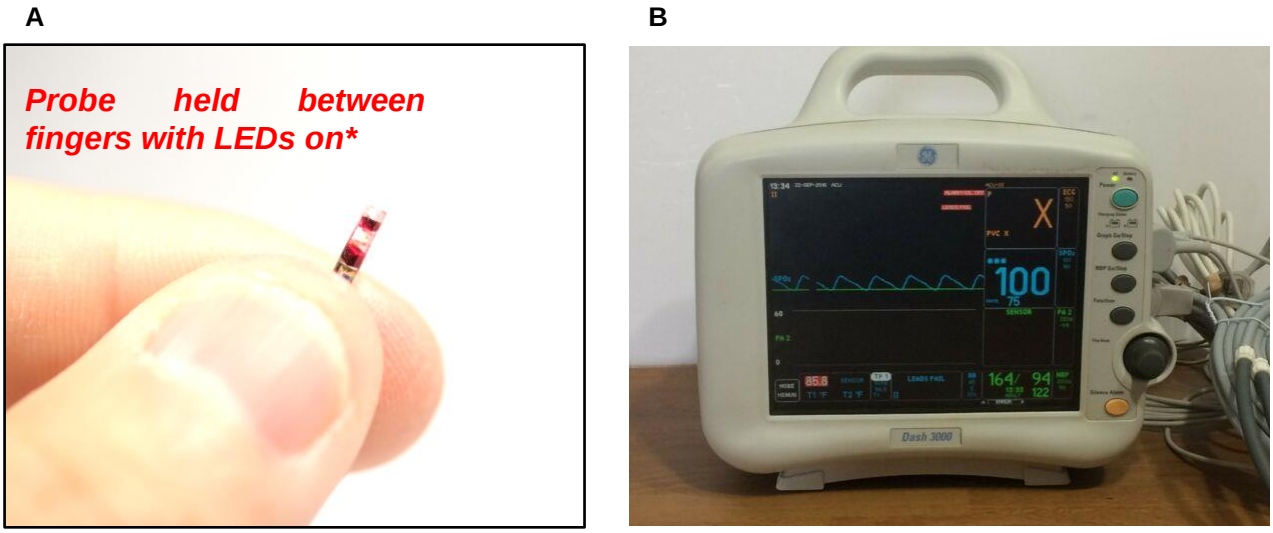

Fig. S16. Measurement method and the test platform for comparing the performance of a wireless catheter oximeter to a clinical standard pulse oximeter. (A) Measurement method of using the wireless catheter oximeter to measure global pulse oximetry. During measurement, the probe is fully covered by the finger. **(B)** A clinical standard pulse oximeter, GE DASH 3000, used in this comparison experiment. (Photo credit: Hao Zhang and Wei Lu, Northwestern University)

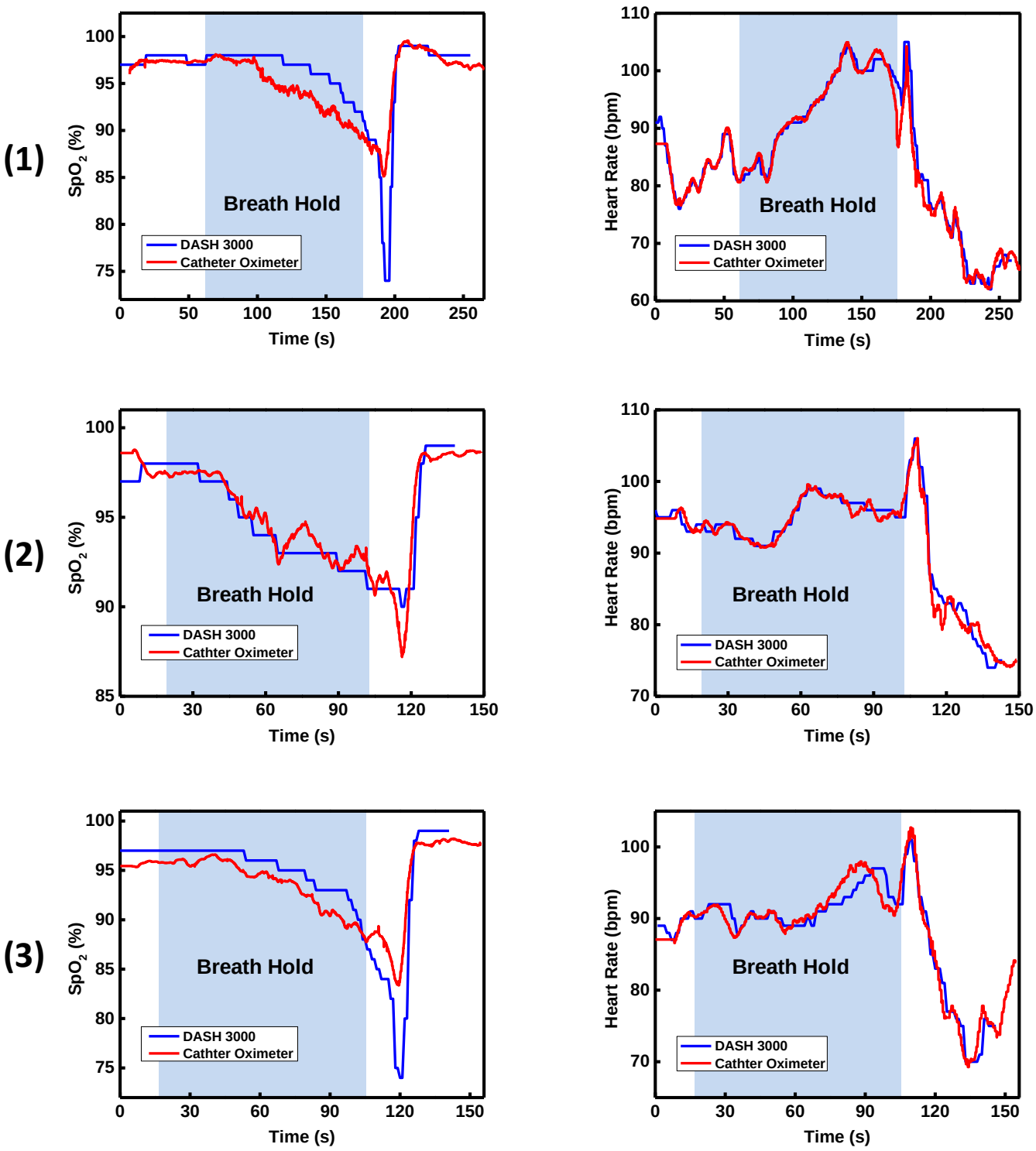

Fig. S17. Additional comparison tests (3 more) between wireless catheter oximeter and clinical standard pulse oximeter. Measured SpO_2 (left) and heart rate (right) from the wireless catheter oximeter attached to the finger during a period of rest followed by a breath hold and then another period of rest, and comparison of the results to measurements performed using a commercial oximeter attached to the other finger (DASH 3000, General Electronics Inc.).

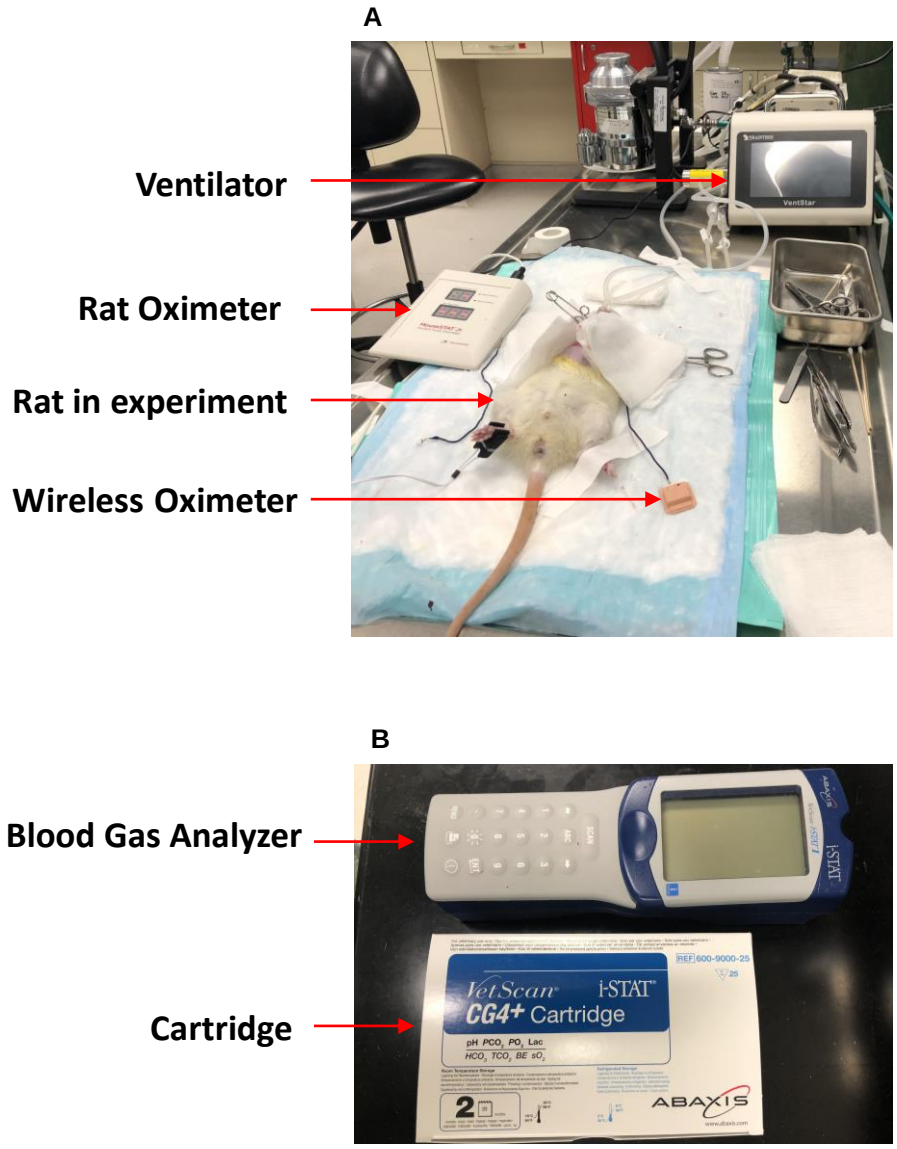

Fig. S18. Animal experiment platform. (A) Animal experiment set up, including an adult female rat under surgery, wireless catheter oximeter, small animal ventilator (Braintree Scientific Inc.), rodent pulse oximeter (MouseSTAT Jr., Kent Scientific Corporation.), blood gas analyzer. **(B)** The blood gas analyzer (VetScan i-STAT 1, Abaxis, Inc.) and the cartridge used in this experiment. (Photo credit: Wei Lu and Zhi-Dong Ge, Northwestern University)

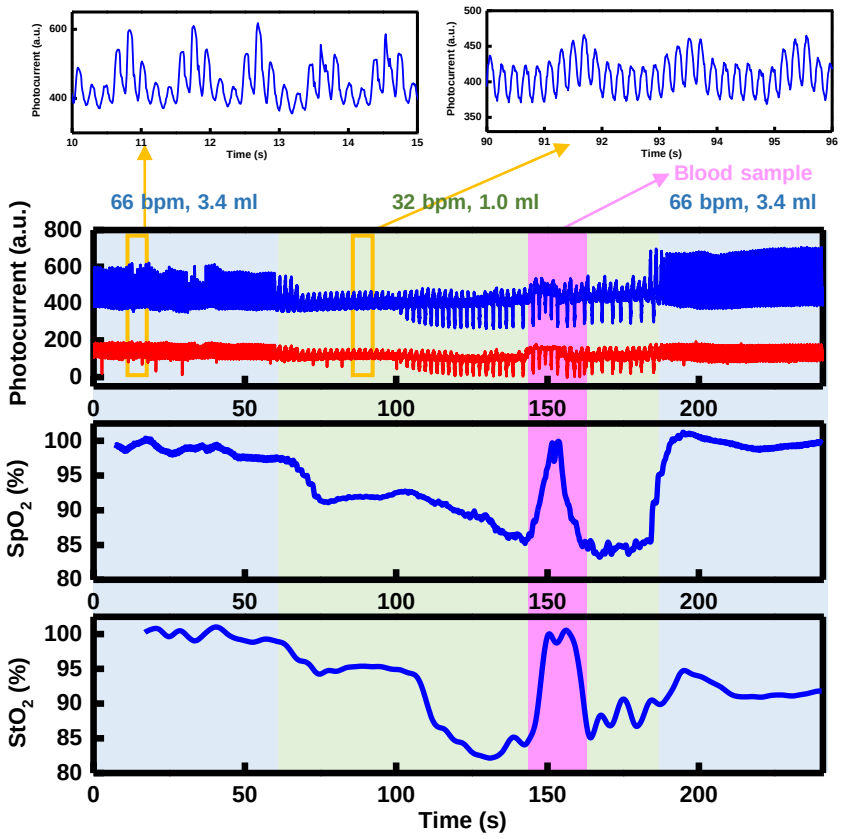

Fig. S19. Raw data and calculated oxygen saturation from a wireless catheter oximeter, recorded from a rat heart during changes in the oxygen supply environment. The left ventricle blood was sampled and measured in the middle of the recording.

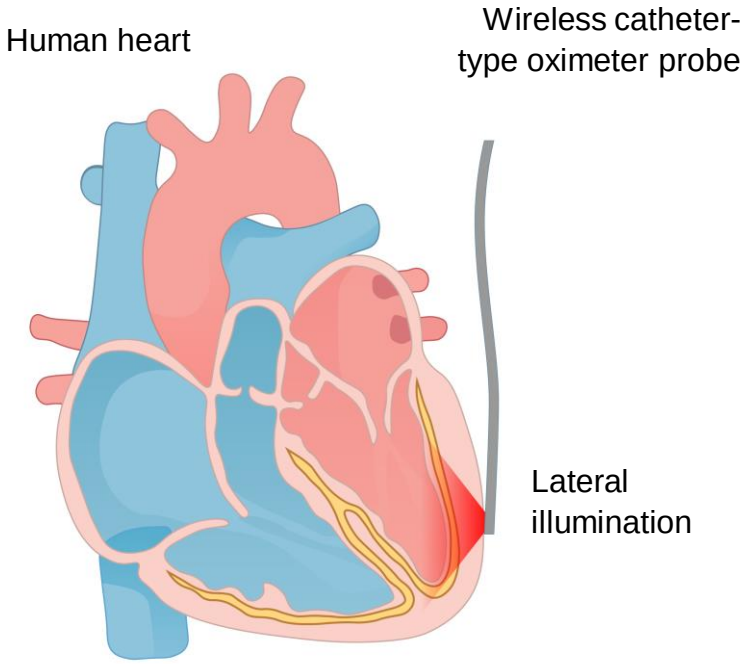

Fig. S20. Schematic illustration of the interface between a catheter-type oximeter probe and the surface of the heart.